Maps of Complex Motion Selectivity in the Superior Temporal Cortex of the Alert Macaque Monkey: a Double-label 2-Deoxyglucose Study

Bard J. Geesaman, Richard T. Born[1], Richard A. Andersen[2] and Roger B. H. Tootell[3]

Massachusetts Institute of Technology, Department of Brain and Cognitive Science, [1]Department of Neurobiology, Harvard Medical School, 220 Longwood Ave., Boston, MA 02115, [2]California Institute of Technology; Division of Biology, Mail Code 216-76, Pasadena, CA 91125 and [3]MGH NMR Center, 149 13th St., Charlestown, MA 02129, USA

The superior temporal sulcus (STS) of the macaque monkey contains multiple visual areas. Many neurons within these regions respond selectively to motion direction and to more complex motion patterns, such as expansion, contraction and rotation. Single-unit recording and optical recording studies in MT/MST suggest that cells with similar tuning properties are clustered into columns extending through multiple cortical layers. In this study, we used a double-label 2-deoxyglucose technique in awake, behaving macaque monkeys to clarify this functional organization. This technique allowed us to label, in a single animal, two populations of neurons responding to two different visual stimuli. In one monkey we compared expansion with contraction; in a second monkey we compared expansion with clockwise rotation. Within the STS we found a patchy arrangement of cortical columns with alternating stimulus selectivity: columns of neurons preferring expansion versus contraction were more widely separated than those selective for expansion versus rotation. This mosaic of interdigitating columns on the floor and posterior bank of the STS included area MT and some neighboring regions of cortex, perhaps including area MST.

The tendency for neurons of similar stimulus selectivity to cluster has been observed throughout the cerebral cortex. In the 1950s, Mountcastle, working in cat somatosensory cortex, found that neurons selective for different sensory submodalities, such as light touch versus deep pressure, were grouped according to response selectivity (Mountcastle, 1957). This organization was columnar, with the axis of the iso-tuning columns oriented perpendicular to the surface of the cortex and extending through the cortical layers. Hubel and Wiesel (1962, 1968) also used single-unit electrophysiology to demonstrate a columnar organization for orientation selectivity and ocular dominance in striate cortex of both the cat and the monkey. Both types of organization were subsequently confirmed and clarified using both 2-deoxyglucose (Hubel *et al.*, 1977; Tootell *et al.*, 1988a,b) and optical recording (Blasdel and Salama, 1986).

Since the seminal works of Mountcastle in somatosensory cortex, and Hubel and Wiesel in visual cortex, a large number of additional 'functional clusterings' have been reported in different species. Several examples have been reported in the macaque: the cytochrome oxidase blobs of striate cortex contain a clustering of neurons with color-opponency, lacking orientation selectivity (Livingstone and Hubel, 1984) and tuned for low spatial frequencies (Tootell *et al.*, 1988c; Born and Tootell, 1989); in the cytochrome oxidase stripes of V2, a segregation of neurons selective for orientation selectivity, end-stopping, color opponency and binocular disparity (Hubel and Livingstone, 1987); in area MT, a columnar organization for direction selectivity (Albright, 1984; Albright *et al.*, 1984); and in inferotemporal cortex, a columnar clustering of neurons tuned for complex spatial features (Fujita *et al.*, 1992). Similar columnar systems have been reported in other species such as the cat (Albus, 1979; Payne *et al.*, 1981; Tolhurst *et al.*, 1981; Berman *et al.*, 1987; Swindale *et al.*, 1987).

The current study explored the functional organization of the superior temporal sulcus (STS), an area of cortex thought to be involved in processing visual motion information (for reviews see Maunsell and Newsome, 1987; Albright, 1993). The most studied region within the STS is area MT, which receives a direct projection from area V1 and contains directionally tuned neurons organized into columns of similar direction preference (Maunsell and van Essen, 1983; Albright, 1984; Raiguel and Orban, 1993; Malonek *et al.*, 1994). Area MT sends a strong projection to the adjacent cortical region, area MST. Many neurons in MST also have motion direction selectivity and are additionally tuned for more complex motion patterns such as expansion, rotation and contraction (Sakata *et al.*, 1986; Tanaka *et al.*, 1986; Duffy and Wurtz, 1991; Graziano *et al.*, 1994; Geesaman and Andersen, 1996).

Previous studies have reported clustering of neurons within area MST according to response selectivity (Duffy and Wurtz, 1991; Lagae *et al.*, 1994). Using single-unit recording and mapping, Lagae and co-workers (1994) have shown evidence that units tuned for expansion, contraction and the two directions of rotation are segregated into separate cortical columns, with columns for expansion and contraction being maximally separated.

We sought to confirm this finding more directly using a double-label 2-deoxyglucose method (2-DG) which exploits the positive correlation between the activity of neurons in a localized region of tissue and the rate of glucose uptake (Kennedy *et al.*, 1975; Sokoloff *et al.*, 1977). By using two different radioactive isotopes of 2-deoxyglucose whose distributions can be recovered independently, the labeling patterns produced by two different stimulus conditions can be compared within the same tissue section (Livingstone and Hubel, 1981; Redies *et al.*, 1987; Friedman *et al.*, 1987, 1989; Tootell *et al.*, 1988a). If a region of cortex is columnarly organized with respect to the stimulus dimension varied between the two conditions, these differences will appear as areas of interdigitation in images where the labeling patterns of the isotopes are compared. For the current experiment, expansion and contraction motions were compared in one monkey; in another monkey expansion and rotation motions were compared.

Materials and Methods

Behavior

Two male rhesus macaque monkeys were used for this study. The animals were trained on a visual fixation task using standard operant conditioning techniques. Scleral search coils and a head post were implanted under general anesthesia and sterile surgical conditions 1 week before training

began so that the eye position could be accurately monitored (Robinson, 1963; Judge *et al.*, 1980).

During training and 2-DG labeling, the animal was seated 57 cm away from a tangent screen and a rear-projection monitor (Zenith) was used to display moving random dots within circular windows subtending 40° of the visual field. The monkey's head position was fixed with a head post. Trials were initiated by the appearance of a green fixation point (0.1°) directly in front of the animal. The center of motion in each stimulus corresponded to the fixation point. Eye position was monitored every 35 ms throughout the trial, and, if eye speeds exceeded 15°/s (indicative of a saccade), the trial was terminated without a reward. The behavioral sequence and data collection were controlled by a PC-compatible 486 computer. Fixation time was continuously monitored during both the training and the 2-DG experiments. To maximize the amount of time that the monkey viewed the visual stimulus, the fixation point and motion pattern remained on the screen as long as the monkey maintained fixation, and the monkey was rewarded with a drop of juice at 3 s intervals. Whenever the monkey broke fixation, the visual stimulus was immediately extinguished (leaving the animal in complete darkness), the reward sequence was turned off and a 2 s time-out was given before the next stimulus presentation. Using this protocol, both monkeys maintained fixation for >85% of the time when isotope was present in the bloodstream during the 2-DG experiments. There were no extended periods of time when the monkeys failed to perform the behavior.

Stimuli

The motion patterns used in this study were identical to those developed by Graziano *et al.* (1994), except that our stimuli subtended larger areas of the visual field (40° in diameter). All stimuli were generated by a PC-compatible 386 computer using a Number Nine (Cambridge, MA) graphics card. These stimuli were limited lifetime random dot motion patterns (Fig. 1), displayed at a refresh rate of 60 Hz. Each panel contained 200 dots within the circular window of the display. The dots remained on the screen for 333 ms (20 frames) before being randomly reassigned to a new position within the display window and a linear trajectory consistent with its new location. The dots were relocated asynchronously, to avoid a coherent flickering of the stimulus. If the dot moved outside the bounds of the display window, it was immediately assigned a random location within the display and a new trajectory. The speed of each dot was a linear function of its distance from the center of the display, given by the formula speed = 0.2 × (distance from the center of the stimulus) per second, the units being arbitrary. The direction of motion for each dot was determined by the type of global motion desired. Expansion required each dot to be moving directly away from the center of the stimulus. Rotation was achieved by turning each of the expansion component motion vectors through 90°. Contraction was achieved by rotating the dots an additional 90° in the same direction. Therefore, one motion type could be transformed into another without any change in the overall velocity distribution – only the global organization of these local motion components changed.

2-DG Double Labeling

For each of two labeling periods, a different visual stimulus was presented to the animal. Macaque #1 viewed expansion motion during the first period and contraction motion during the second. For macaque #2, a counter-clockwise rotation motion pattern was presented during the first labeling period (^{3}H), lasting 45 min, and expansion motion during the second period (^{14}C).

In both animals, the time course of the labeling experiments was as follows: the monkey viewed the first pattern for 5 min before the i.v. injection of the first label (always ^{3}H), to ensure that he would consistently perform the behavior before committing to the procedure. After gradual injection of the [^{3}H]DG (2-[1,2-^{3}H]deoxyglucose, 13.6 mCi/kg body wt; 40 Ci/mmol sp. act.), the i.v. line was slowly flushed with 4 ml of normal saline. After 45 min, the visual stimulus was changed and the [^{14}C]DG label (2-[1-^{14}C]deoxyglucose, 17 μCi/kg body wt; 54 mCi/mmol sp. act.) was injected. After a 10 min exposure to this second pattern, the monkey was killed by pentobarbital overdose (>50 mg/kg, to effect) and then perfused through the heart with saline followed by fixative (2.25% glutaraldehyde with 0.5% paraformaldehyde).

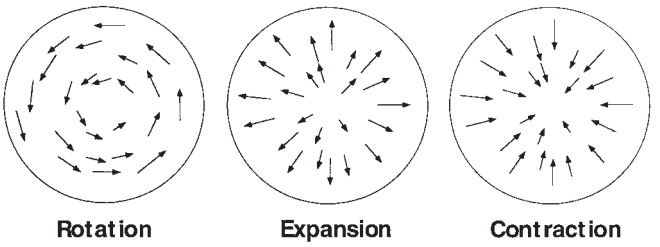

Figure 1. Complex motion pattern stimuli. Random dot patterns of rotation, expansion and contraction. Monkey 2 viewed rotation during the first labeling period and expansion during the second. Monkey 1 viewed expansion for the first labeling period followed by contraction. All patterns were viewed with the fixation point centered in the middle of the pattern. Details of how these stimuli were constructed are provided in the text.

The 45 min exposure for the first condition followed by a brief 10 min exposure for the second condition departs from the optimal total experimental duration of 45 min established by Mori *et al.* (1990). This optimal duration of 2-DG uptake represents the amount of time during which most of the injected DG is taken up from the bloodstream. However, if one perfuses the experimental animals (Tootell *et al.*, 1982, 1988b), excess unlabeled DG is washed out, eliminating cross-contamination from unbound DG in the bloodstream, and excellent labeling can be obtained within relatively short periods (Tootell *et al.*, 1982, 1988b). In calibration tests we established that robust activity labeling was obtained after only 10 min. We used this stimulation interval for the second label in subsequent double-labeling procedures in order to minimize the possibility of recirculation of the first (^{3}H) isotope (because small amounts of label leave the cell over time).

The brain was removed, dissected and frozen within 5 min of the pentobarbital infusion. The two hemispheres were separated: the left hemisphere was frozen intact by placing its medial surface on a metal block chilled with dry ice, and the right hemisphere was unfolded and flattened before being frozen (Tootell and Silverman, 1985). Both isotopes were purchased from American Radiochemicals Corp. (ARC), St Louis, MO.

Forty-micron thick sections were cut on a cryostat, mounted onto subbed coverslips, dried and then apposed to film to obtain autoradiographs. Two different films were used: to visualize the ^{3}H signal, sections were exposed on ^{3}H-sensitive Hyperfilm (Amersham) for 1 month at –80°C. Subsequently, the film was developed by immersion at 10–12°C in Kodak D-19 developer for 5 min followed by a stop bath for 30 s and finally fixed with Kodak Rapid Fix for 4 min. To obtain the ^{14}C images, a color transparency film (Polaroid 891) was exposed for 3–4 months at –80°C. This film was developed using a Polaroid dry processor.

Data Analysis

Several modifications of previous methods (Friedman *et al.*, 1987, 1989; Juhler and Diemer, 1987) were used to recover independent labeling patterns for the two isotopes. Color film and Hyperfilm were used to recover the ^{14}C and ^{3}H labeling patterns respectively. When exposed on color film, the two isotopes of 2-DG interact differently with the three emulsion layers. The lower energy beta particles emitted by tritium penetrate only the most superficial (blue) layer; the higher energy ^{14}C beta particles penetrate all three layers. Using a yellow filter, which blocks the contribution of the blue layer, an isolated image of the ^{14}C labeling pattern was obtained. Because much more ^{3}H than ^{14}C label was used for this study, the Hyperfilm (^{3}H-sensitive) autoradiographs largely reflected the distribution of tritium label.

For this study, we used a larger ^{3}H:^{14}C ratio than most investigators. In pilot studies, we began our calibration tests (unpublished data) using the ratios in the literature (i.e. 50–100:1), but used two independent criteria to determine whether these ratios actually yielded optimal isotope seperation. These two independent criteria were: (i) directly comparing autoradiograms using visual stimulation, which produced predictably different topography of activation (retinotopic differences, ocular dominance columns in different portions of the visual field, etc.); and (ii)

the use of color film to indicate which isotope was producing which images (i.e. saturated blue images from the ^{3}H, and reddish-white on the same film produced by ^{14}C). These calibration tests (and companion tests using methacrylate standards on the same films) indicated that the published ratios were biased towards the ^{14}C (i.e. not enough tritium label was used), at least with our combination of films, slice thickness and other experimental conditions. In subsequent experiments in animals using the same approach, we systematically increased the ratio of ^{3}H:^{14}C until the effects were more differentiable. The optimal ratio we used was 800:1, a ratio which has consistently differentiated different kinds of columns and retinotopic patterns in ~30 monkeys to date. Our own unpublished data from calibration experiments revealed that, at the ^{3}H:^{14}C isotope ratio of 800:1 used in the current experiment, the contamination of the tritium signal by ^{14}C amounted to no more than 10%.

The images from all autoradiographs in the current study were digitized using a CCD camera, then imported into NIH Image where sequential sections were averaged together in order to improve the signal-to-noise ratio and to correct for laminar variation. We were careful to align successive images using features present in the isotope patterns. The alignment of single sections was performed manually, using an on-line comparison of images taken from the same tissue section. First, the images were mounted at the same focal/magnification plane on a modified microscope mechanical stage which allowed independent, fine-scale adjustments in the x, y and rotation axes. A stored image of the autoradiograph from one film type was presented at half-transparency, while an image from the second film type was also presented at half-transparency – thus allowing on-line alignment of the two images. Contrast of either image could be inverted (when tissue sections were in alignment, this would null out the borders and tissue artifacts in the two sections), or presented at the same contrast (so that the image borders and artifacts from the two sections would combine when aligned). Empirically, presenting the two sections in opposing contrast tended to yield the most robust alignment effects, as one might expect from the nonlinear perception of contrast in psychophysical studies. This comparison was done at a magnification of ~8 μm per pixel, using images of 520 × 480, so that alignment innaccuracies could not have been greater than 1 or 2 pixels without having an obvious effect on the image. When the two images were out of alignment in the rotation axis, this led to immediate and obvious 'Glass Pattern' effects. When the two images were out of alignment in the x and y axes, this produced an equally obvious 'double image' which could be immediately corrected by minor readjustment of the mechanical stage. This same method was used both when averaging consecutive images of the same isotope and for producing difference images of the two isotopes. When more than two images were averaged, this method was used both between consecutive image slices and with image slices throughout the series being averaged. The patterns of interdigitation in the difference images were in all cases consistent with the gross impression obtained by lining up the image negatives on a light box. Major results were checked by two independent operators.

In regions of the brain where a columnar organization was evident on the individual autoradiographs, the spatial relationship between the labeling patterns was visualized by digitally subtracting the gray-level ^{14}C image from the ^{3}H image, after the two images were equated for average pixel luminance and contrast range. The resulting difference images had intermediate density values (appearing gray) in regions of tissue where the two labeling patterns were in register and interdigitating white and black columns where they were out of phase.

Computing Local Phase Difference

We developed an algorithm for comparing periodic images that quantified the degree of overlap between the two patterns by calculating relative phase. By convention, image regions 0° out of phase maximally overlap; regions 180° out of phase interdigitate maximally. Although obtaining relative phase is straightforward for two-dimensional sine wave gratings, it is nontrivial for autoradiographs of varying periodicity, varying phase difference and containing a considerable amount of noise in the data.

Our method takes two autoradiograph images as input and produces a topographically aligned two-dimensional array that expresses the local phase difference for each point in the original autoradiographs. This 'phase map' represents the degree of overlap for each local region of the tissue slice.

To perform this computation, the two gray-scale input images are stored as two-dimensional arrays of pixels, indexed according to gray level. A square neighborhood centered about each location is sampled in the two images. The larger the neighborhood, the less sensitive the algorithm is to noise, but this is acheived at the cost of spatial resolving power. These two arrays are multiplied together pixel by pixel and then summed to get a scalar. As in cross-correlation, the degree of correspondence between the two arrays is reflected in the magnitude of this number. This follows from the result that the sum:

$$\sum_{i=0}^{n} p_i q_i$$

is maximized when **p** and **q** (the two series of numbers obtained by transforming the s by s arrays being compared into vectors $s \times s$ values long) are sorted such that the ith largest number in p is multiplied by the ith largest number in **q**. This sum is minimized when the ith largest number in **p** is multiplied by the $(n - i)$th largest number in **q**.

The output of the above operation depends not only on the degree of correspondence between the two neighborhoods but also on overall image brightness and contrast. Relative phase needs to be independent of these characteristics. To accomplish this, the output of the algorithm was normalized by linearly mapping the result onto the space bounded by the minimum and maximum solutions to the above summation, where series **p** and **q** were obtained from the pixel values of the neighborhoods under consideration. In the convention used to represent our images, a value of 0 indicates maximal interdigitation and a value of 1 indicates maximal overlap. For example, comparing neighborhoods [2 1; 3 4] and [1 2; 4 3], unscaled output = (2 × 1 + 1 × 2 + 3 × 4 + 4 × 3) = 28; min summation = (1 × 4 + 2 × 3 + 3 × 2 + 4 × 1) = 20; max summation = (1 × 1 + 2 × 2 + 3 × 3 + 4 × 4) = 30; normalized output = (28 – 20)/ (30 – 20) = 0.8 (phase difference of (1 – 0.8) × 180 = 32°).

Before running the algorithm on real data, simulations using pairs of two-dimensional sine wave gratings confirmed that our filter was insensitive to image contrast, average luminance, and pattern frequency. However, it was relatively sensitive to noise. Adding as little as 10% 'salt and pepper' noise (randomly assigning 10% of pixels to black or white) to the input images markedly degraded the performance of the algorithm. With 40% added noise, the output signal was reduced to almost zero. By smoothing the noisy images with a Gaussian filter at the input stage, performance was markedly improved, with only modest reduction in performance with as much as 60% added noise. A two-dimensional Gaussian filter with a standard deviation of 3 pixels proved optimal for reducing image noise without significantly reducing signal. In the analysis of real images, this filter was applied to the data before further processing.

Figure 2 shows the relationship between relative phase and the output of the filter. These data were obtained by running two-dimensional sine wave gratings of known phase difference through the algorithm. Before processing, each test image was degraded with 40% 'salt and pepper' noise to make the simulation more realistic. Except at the extremes of phase difference, the output has the desired property of being relatively linear.

For simulations using sine wave gratings of constant phase difference and no noise, the size of the neighborhood used as the kernel had little effect on the output array. For real images, larger kernels are less sensitive to noise but decrease the resolution at which local changes in relative phase can be detected. For this study, we chose a kernel size approximately equal to the period of the labeling pattern (15 pixels) and found empirically that this represented a good compromise between noise tolerance and spatial resolving power.

Relative phase is undefined for areas of tissue that contained neither label. The ^{14}C and ^{3}H isotope maps were summed and the resultant image thresholded below an arbitrarily assigned value so that tissue with little or no label of either kind appeared black. These regions were then applied as a black mask over our pseudo-color maps.

Because it computes local relative phase, this filter could work as a crude machine-vision algorithm for stereo-vision (Sanger, 1988).

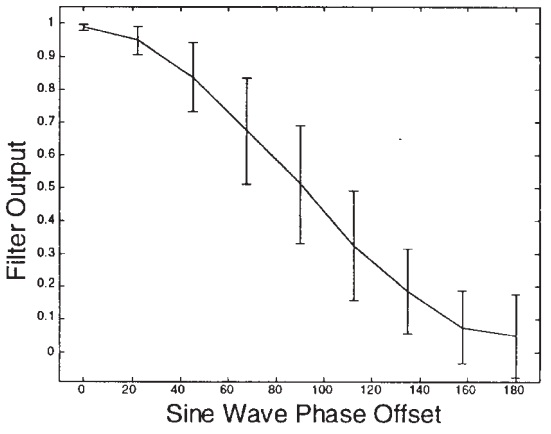

Figure 2. Calibration function for local phase algorithm. This graph shows the output of our local phase algorithm as a function of the phase difference between input images. The data for this figure were obtained by running simulations using two-dimensional sine wave gratings of various, known phase offsets. Because the phase difference was constant over each input pair, the output was a relatively homogeneous two-dimensional array. The mean and standard deviation were calculated for each of these data sets and plotted in the figure. Note that the function has the desired behavior of being relatively linear, except at the extremes of phase. In order to better simulate real-world conditions, 40% salt-and-pepper noise was added to the test images before filtering.

Results

Both the ^{3}H and ^{14}C autoradiographs demonstrated a number of labeled columns in several diverse regions of cortex. We found columnar labeling in auditory cortex, throughout regions of the inferior parietal sulcus, in areas V2 and VP, as well as in the STS. These columns were oriented orthogonal to the surface of the cortex and extended through most or all cortical layers, with densest labeling in the middle layers. These columns were generally 0.2–0.5 mm in diameter, although the spacing between the columns varied more widely.

Although columnar labeling was found in diverse areas of cortex, the patterns of ^{14}C and ^{3}H exposures superimposed in all regions examined, except for parts of the floor and posterior bank of the STS. Within the STS, extensive regions of non-overlapping, columnar labeling were evident on the two sets of films (Figure 3). Panels *A* and *B* of Figure 3 show individual exposure patterns for the ^{14}C and ^{3}H isotopes respectively. Panel *C*, which is the difference of the patterns in panels *A* and *B*, clearly shows interdigitating columns indicative of a columnar organization. These images were obtained from macaque #1, where expansion and contraction patterns were compared. Panel *E* is the difference image in false-color, with green representing areas of ^{3}H label (expansion) and red ^{14}C label (contraction). Yellow regions of this image represent cells which responded to both motion patterns, while black image areas contained cells which responded to neither stimulus. Before the false color was applied, the gray-scale image of panel *C* was put through a difference-of-Gaussians filter (sd1 = 8 pixels; sd2 = 20 pixels; kernel = 50 pixels) in order to smooth noise and emphasize the transitions between cortical columns.

Figure 4 shows ^{3}H and ^{14}C autoradiographs of the corresponding STS anterior bank sections, along with their difference image. By referring to the scale bar for each image, it is apparent that the labeled columns on the anterior bank were poorly defined and large, and nearly superimpose for the two different isotope maps.

Figure 5 shows a horizontal section of the STS through both MT and MST from the right hemisphere of the same monkey. Panels *A* and *B* show the distributions of ^{14}C and ^{3}H label, respectively, and panel *C* is the difference image. Consistent with the flattened sections, the roughly columnar pattern in all three of these images is much more evident on the floor and posterior bank of the sulcus. The difference image shows no signs of columnar interdigitation extending onto the anterior bank.

Phase Relationships

In Materials and Methods we described another way of examining this relationship by calculating local relative phase. Figure 3*F* shows the result of applying this algorithm to the autoradiographs of the floor and posterior bank of the STS from macaque #1 (expansion-versus-contraction). The blackened areas of these figures correspond to regions of tissue where both ^{14}C and ^{3}H signals were weak and the phase offset was consequently undefined. Although regions of maximum offset correspond to the area of interdigitation present in Figure 3*C*, this phase relationship is not constant within any extended region of cortex. Within the area of interdigitation exist local areas where the ^{14}C and ^{3}H images superimpose, as would be expected for columns of neurons having motion preferences orthogonal to those tested. Table 1 summarizes the average phase offsets for several cortical areas for one monkey. For example, in the area of cortex labeled as area MT in Figure 3, the average phase offset was 93°. Within cortical areas V4t, V2/V3a and the anterior bank of the STS, the average phase differences were considerably less.

The double label experiment was repeated with a second monkey, macaque #2. In this experiment, expansion and rotation motion were compared (locally, motion was 90° apart rather than 180°, as in macaque #1), phase differences were considerably less pronounced, consistent with the decreased difference in local stimulus direction. The average local phase difference in the region of interdigitation on the floor of the superior temporal sulcus corresponding to areas MT and MST was only 58° in macaque #2, compared with 93 and 104° in areas MT and MST, respectively, in macaque #1 (Table 1). Because the pattern of interdigitation in macaque #2 was much less distinct, the borders between anatomical areas were difficult to determine, which is why we lumped together phase data for MT and MST in this monkey. As in the first monkey, the anterior bank for this macaque lacked differential labeling.

We could not definitely assign the region of interdigitation on the floor and posterior bank of the STS to any single anatomical area, although the major area of interdigitation occupies a portion of the posterior bank of the STS previously identified as area MT. We have superimposed tentative borders for this oval-shaped cortical region over the 2-DG difference map in Figure 3*D*. Figure 6 (after figure 1 in Desimone and Ungerleider, 1986) depicts the cortical areas within the STS mapped using a combination of single-unit recording and anatomical techniques. As labeled in Figure 3*D*, additional interdigitated regions extending beyond tentative MT on the fundus of the STS correspond to areas previously identified as area MST. Based on these previous studies, the oval patch of cortex in Figure 3 devoid of label and adjacent to the anterior edge of the interdigitating pattern is probably the far peripheral representation of MT (MTp) (Ungerleider and Desimone, 1986). Because the motion patterns that the monkeys viewed were limited to the 20° of the visual field on either side of the fixation

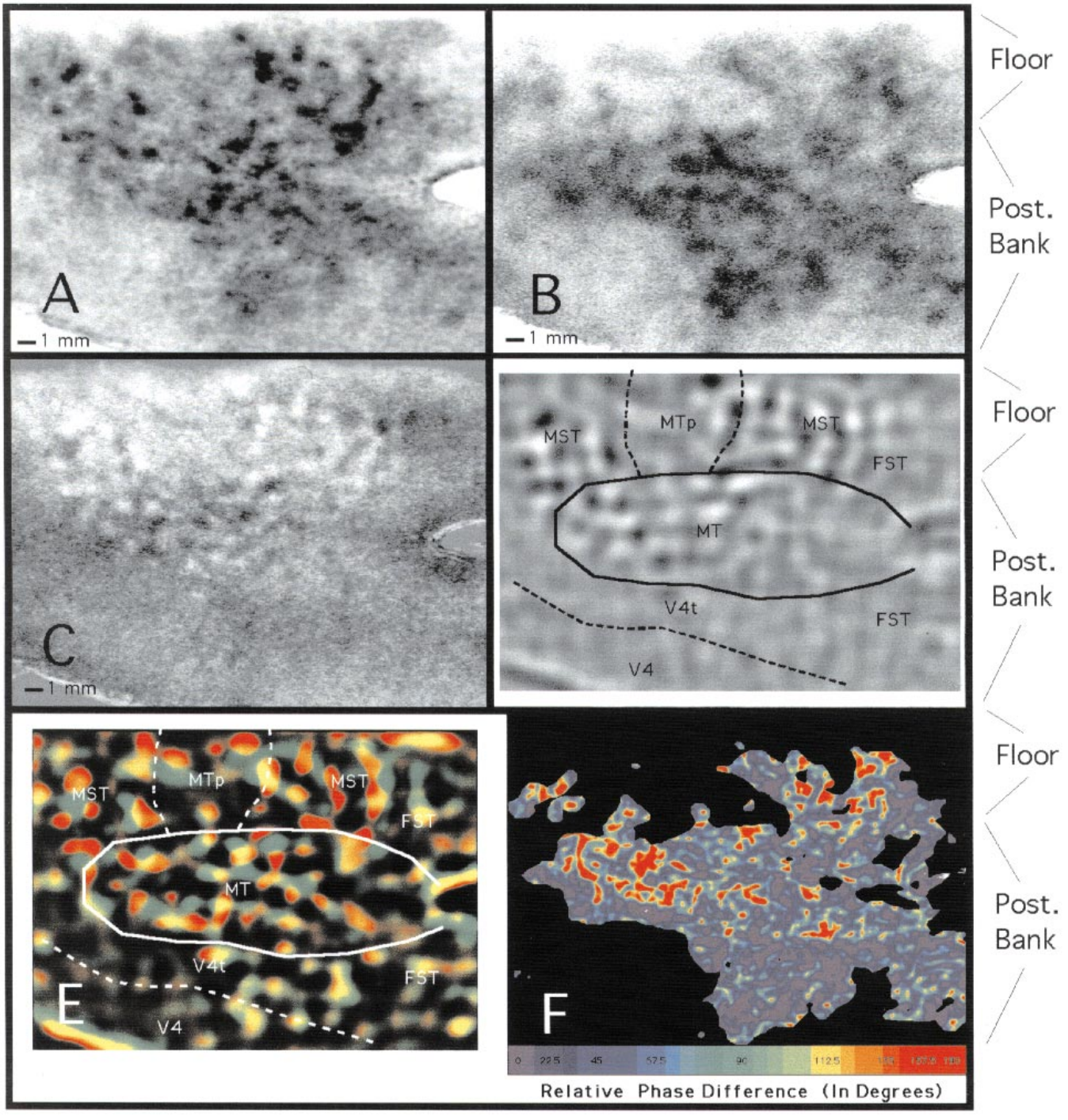

Figure 3. Autoradiographs from flattened tissue sections and difference images of the posterior bank and floor of the STS. (*A*) ^{14}C label. (*B*) ^{3}H label. (*C*) Difference image. (D) Approximate anatomical borders superimposed over the image from *C*. This image was enhanced using a difference of gaussians filter. The periodicity produced within the non-interdigitating portions of *D* is an artifact of the filter. (*E*) False-color difference image. (*F*) False-color phase map of the STS floor and posterior bank from macaque #1. Differential labeling was seen both in area MT and in the two regions which extend onto the floor of the STS. Although there was strong ^{3}H and ^{14}C labeling in neighboring regions such as V4t, the two patterns largely superimposed and the signal was absent in the difference image. The top border of this section is continuous with the border of the section shown in Figure 4. See Figure 5 for a horizontal section through this same region of cortex, from the contralateral hemisphere. The phase map in *F* was constructed using the ^{14}C and ^{3}H images from *A* and *B*. The region of maximum phase difference (red) corresponds well to regions of interdigitation seen on the difference map of *C* and *D*. However, the phase difference within the region of interdigitation varies considerably — there are regions with MT proper where the labeling pattern is 'in phase', as would be expected for columns of neurons that responded similarly to these specific motion stimuli. The color legend at the bottom of the figure was constructed based on the calibration curve of Figure 2. In this color scheme, violet represents a phase difference of 0° and red 180°. All images are to the same scale; the images in frames *E* and *F* are smaller because image edges were not zero-padded before convolution.

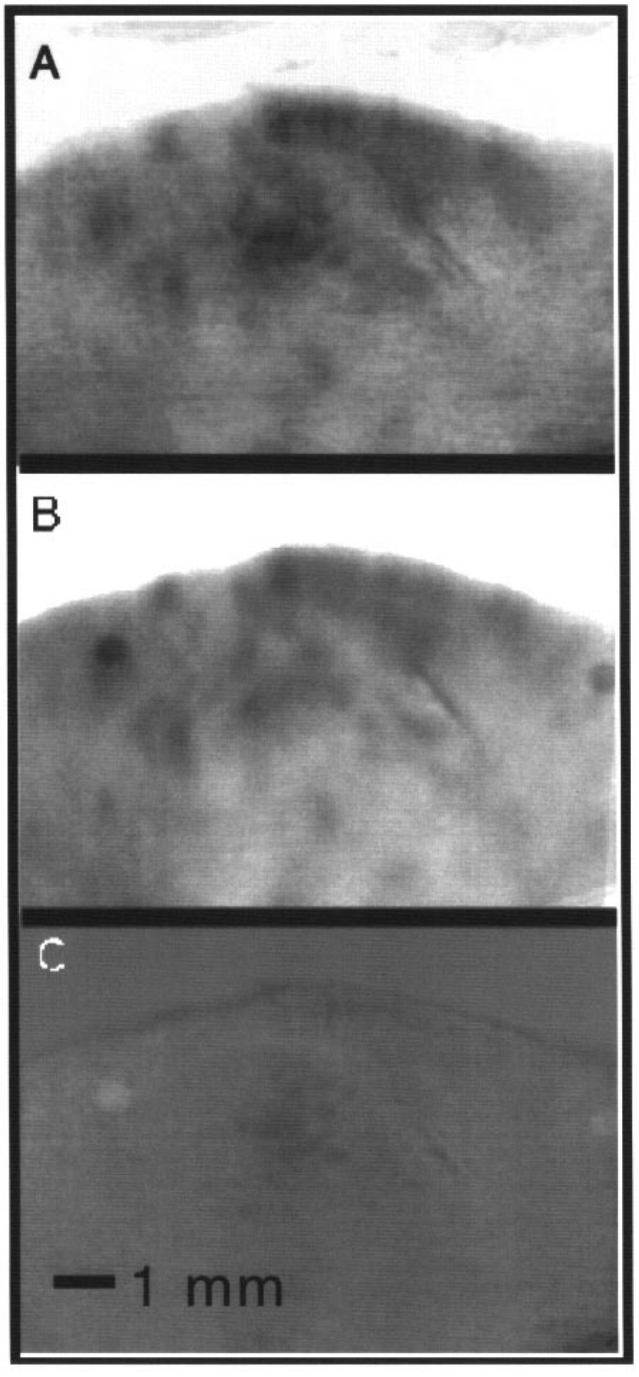

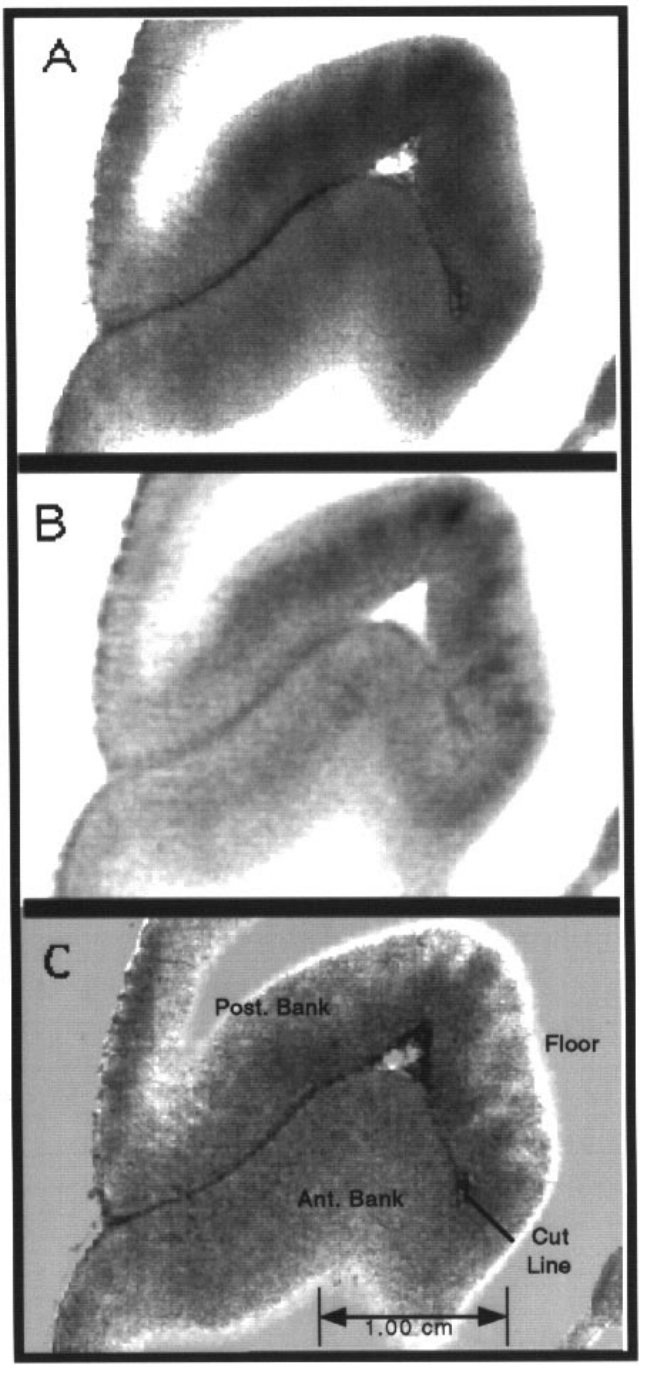

Figure 4. Autoradiographs from flattened tissue sections and difference images of the anterior bank of the STS. (*A*) ^{14}C label. (*B*) ^{3}H label. (*C*) Difference image. Note that the two labels nearly superimpose (in phase). The scale is the same as in Figure 3. The tissue from Figures 3 and 4 directly adjoin and were separated while preparing the sections.

Figure 5. Cross-sections of the STS, including areas MT and MST. Autoradiographs come from the unflattened (right) hemisphere of macaque #1. (*A*) ^{14}C label. (*B*) ^{3}H label. (*C*) Difference image. The posterior bank is towards the top of each panel. The cortex surface is towards the left. Note on the difference image that the region of interdigitation ends just before the anterior bank. This is consistent with the flattened sections of Figures 3 and 4. *C* shows the approximate location of the cut that separated the tissue from Figures 3 and 4.

point, regions of cortex containing cells with receptive fields in the far periphery should be unlabeled. The two flanking regions of interdigitation have tentatively been assigned MSTd and MSTl, consistent with the Desimone and Ungerleider map. This assignment is also consistent with boundaries between visual areas within the STS defined by labeling cortical regions corresponding to the vertical and horizontal meridia. This was done using the same double-label 2-DG methodology described here, but in the anesthetized macaque (Tootell and Born, 1990).

Table 1. Average phase differences between ^{3}H and ^{14}C autoradiographs from different visual areas

Cortical area	Phase difference (°)
MT	93
MST	104
STS ant. bank	56
V4t	48
V2/V3	26
STS floor (macaque 92-1)	58

All values are for macaque #1 (expansion-versus-contraction) except the last entry (expansion-versus-rotation in macaque #2). Values were calculated according to the local phase algorithm described in the text.

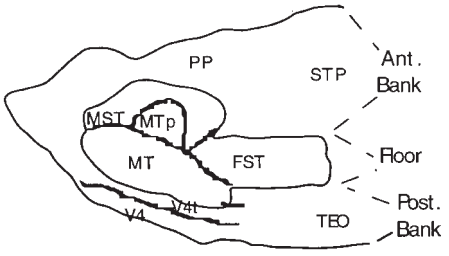

Figure 6. Map of the STS showing multiple cortical areas, taken from Desimone and Ungerleider (1986), constructed using a combination of single unit recording and myelin staining.

Discussion

We have shown evidence that neurons tuned to motion are organized into distinct cortical columns within the STS of the macaque monkey.

Tuning Specificity

Areas of interdigitation in the difference image correspond to regions of cortex where anatomically distinct populations of neurons responded differently to the two stimulus patterns. Such a pattern does not necessarily reflect a functional organization with respect to *complex* motion per se. For example, although area MT has not been shown to possess neurons selective for these patterns, differential labeling occurred in this study because of these cells' specificity for local linear motion. This is because the receptive fields in MT cells are small compared with the 40° diameter stimulus patterns used in this study, so that the portion of the stimulus viewed by a single MT cell contained approximately linear motion (Figure 7). Thus in the experiment where we compared expansion with contraction, an MT neuron whose receptive field was located above the fixation point would 'see' essentially linear upward motion during the first condition and linear downward motion during the second. This is particularly true for those neurons with receptive fields near the periphery of the stimulus. As a result, the interdigitation seen within area MT most likely reflects the previously proposed organization with respect to *linear* motion (Albright *et al.*, 1984).

This caveat might also apply to the interdigitating columns seen in area MST; however, given the large receptive field sizes of neurons in this area and previous demonstrations that neurons here are indeed tuned for complex motion patterns, we feel it is much less likely. Instead, we interpret the patterns found on the floor of the STS to be the first anatomical evidence for a columnar organization of neurons selective for complex motion patterns.

Figure 7 makes the additional point that the pattern of labeling

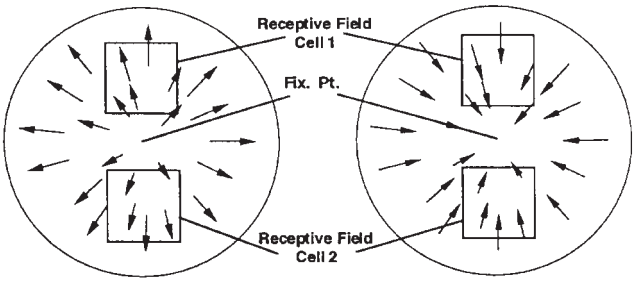

Figure 7. Complex motion patterns and linear receptive fields with the same directional tuning but different retinotopy. An MT neuron tuned for linear motion with a small receptive field will respond to the directional motion components of complex motion patterns. Although tuning to linear motion is the same for the two cells, tuning for complex motion patterns depends on the placement of the stimulus. As explained in the text, DG labeling patterns depend on receptive field size, tuning specificity and location of the receptive field.

is influenced both by the selectivity of the cell and the location of the cell's receptive field with respect to the stimulus. In this schematic model, both cells are tuned for upward motion. The cell with its receptive field above the fixation point responds well to the expansion pattern but poorly to the contraction. The cell below the fixation pattern has the opposite response, although the two cells share the same tuning specificity. Therefore, the labeling patterns we obtained in MT were determined both by tuning selectivity and retinotopy.

Direction Columns

Directly relevant to this study are reports of directional selectivity in the superior temporal sulcus. Using single-unit mapping of this region, Albright *et al.* (1984) found a clustering of units with similar response selectivity in area MT. Similar to the arrangement in striate cortex for orientation, they found that, moving tangential to the cortical surface, direction preference changes gradually, with periodic 180° reversals in the preferred direction. Based on these data, they suggested that cells with similar directional tuning are organized into con- tinuous slabs of cortex aligned normal to the pial surface.

Our study generally supports Albright's proposed functional organization for MT. Because our stimuli are large compared with the size of an MT neuron's receptive field, during labeling these cells viewed essentially linear motion through the aperture of their receptive fields. The component motion vectors were essentially perpendicular to one another for the case of expansion and rotation and were oriented 180° apart for expansion and contraction. Our results are therefore consistent with those obtained in the anesthetized macaque by Tootell and Born (1991) using translational motion and double-label DG techniques. They found that an interdigitating mosaic of columns in area MT was best obtained using motion patterns of opposite directionality.

With the stimulus patterns used in this study, the calculated phase difference within MT/MST was always much less than 180°. Failure to achieve perfect interdigitation is explained by Figure 3*E*, which shows areas within MT/MST that did not respond to either pattern. Some of these unlabeled subregions potentially represent interbands within the band/interband architecture reported in area MT (Born and Tootell, 1992). MT interbands respond well to small motion patterns but poorly to large stimuli, such as those used in the current study. In support of this explanation, when our phase algorithm was applied to 2-DG images of area MT from a unpublished study which used

small, linear motion patterns, the average phase difference approached 180°.

Significance of Cortical Columns

The images obtained in this study lend further support to the hypothesis that mammalian cortex is organized into anatomical columns that are composed of functionally discrete subunits (for a review see Tootell *et al.*, 1993). As is typical (but under-reported in DG studies), we saw evidence of columnar organization throughout diverse regions of the brain, including auditory cortex, somatosensory cortex and visual cortex, although we found a systematic representation of motion pattern only on the posterior bank and floor of the superior temporal sulcus.

Organizing cortex into functional columns decreases the wiring complexity of establishing connections between different neurons, because neurons with similar response profiles and receptive field locations make similar types of connections (Cowey, 1979; Nelson and Bower, 1990; Mitchison, 1992). Along these lines, these authors have argued that dividing the brain up into different anatomic regions and further breaking up these regions into discrete functional subunits (Mitchison, 1992) minimizes wiring volume. Clustering units of similar specificity together also facilitates the formation of local circuits via the dendritic processes of projection neurons and the processing provided by local interneurons (Tootell *et al.*, 1993). Shadlen and Newsome (1994) have argued that the intrinsic noisiness of a single neuron's rate code requires redundancy to smooth out this variability. Clustering neurons of similar specificity into cortical columns is an efficient way of introducing this redundancy without further increasing the complexity of the wiring.

The apparent columnar organization for complex patterns of motion within area MSTd has interesting implications for the mapping of space using optical flow motions. Bradley *et al.* (1996) have recently shown that area MSTd neurons adjust their focus tuning to compensate for eye movements, providing strong evidence that MSTd activity codes the heading for navigation, regardless of whether the eyes are stationary or moving. Britten (1996) has found that microstimulation of expansion columns within MSTd can bias a monkey's perceived heading direction. These experiments suggest that the complex-motion columns within area MSTd may comprise a functional map of space derived from optical flow information.

Final Comments

There are several advantages of combining two activity labels in awake-behaving monkeys. First, there is always the concern that the response profiles of cells may change under anesthesia, making generalizations to the awake animal tenuous. Specifically, cortical activity has been shown to be suppressed under the influence of anesthesia and the metabolic rate throughout the gray matter becomes more uniform (Sokoloff, 1977; Sokoloff *et al.*, 1977). Another advance of this study was the more perfect separation of the two 2-DG labeling pattern using techniques described in the Materials and Methods section.

In conclusion, using the 2-DG double labeling technique we have demonstrated the presence of a columnar organization in areas of cortex sensitive to complex motion patterns such as expansion, rotation and contraction. We were able to visualize this organization with isotope maps labeling cells of known specificity. This interdigitation was more pronounced for expansion/contraction than expansion/rotation, suggesting that units driven by expansion and contraction patterns are maximally separated across the surface of the cortex, as one would expect from a 360° mapping of local or global direction. We have argued, based on retinotopy and the pattern of periodic labeling evident on difference images, that the area of interdigitation partially overlaps both regions MT and MST.

Notes

The authors would like to thank Gail Robertson for excellent technical assistance and Ning Qian for a discussion of the local phase algorithm. This project was support by NIH grants RO1 EY07492 (R.A.A.), RO1 EY11379 (R.T.B.) and RO1 EY07980 (R.B.H.T.), and the Human Frontiers Science Program (R.A.A. and R.B.H.T.).

Address correspondence to: Roger B. H. Tootell, MGH NMR Center, 149 13th St., Charlestown, MA 02129, USA.

References

Albright TD (1984) Direction and orientation selectivity of neurons in visual area MT of the macaque. J Neurophysiol 52:1106–1130.

Albright TD (1993) Cortical processing of visual motion [Review]. Rev Oculomot Res 5177–5201.

Albright TD, Desimone R, Gross CG (1984) Columnar organization of directionally selective cells in visual area MT of the macaque. J Neurophysiol 51:16–31.

Albus K (1979) ^{14}C-Deoxyglucose mapping of orientation subunits in the cats visual cortical areas. Exp Brain Res 37:609–613.

Berman NE, Wilkes ME, Payne BR (1987) Organization of orientation and direction selectivity in areas 17 and 18 of cat cerebral cortex. J Neurophysiol 58:676–699.

Blasdel GG, Salama G (1986) Voltage-sensitive dyes reveal a modular organization in monkey striate cortex. Nature 321:579–585.

Born RT, Tootell RBH (1989) Spatial frequency tuning and surround inhibition of single units in macaque supragranular striate cortex. Ophthalmol Vis Sci (Suppl) 30:111.

Born RT, Tootell RBH (1992) Segregation of global and local motion processing in primate middle temporal visual area. Nature 357:497–499.

Bradley DC, Maxwell M, Andersen RA, Banks MS, Shenoy KV (1996) Mechanisms of heading perception in primate visual cortex. Science 273:1544–1547.

Britten KH (1996) Microstimulation of extrastriate area MST influences heading judgements in monkeys. Soc Neurosci Abstr 22:1692.

Desimone R, Ungerleider LG (1986) Multiple visual areas in the caudal superior temporal sulcus of the macaque. J Comp Neurol 248:164–189.

Duffy CJ, Wurtz RH (1991) Sensitivity of MST neurons to optic flow stimuli. I. A continuum of response selectivity to large-field stimuli. J Neurophysiol 65:1329–1345.

Friedman HR, Bruce CJ, Goldman-Rakic PS (1987) A sequential double-label ^{14}C- and ^{3}H-2-DG technique: validation by double-dissociation of functional states. Exp Brain Res 66:543–554.

Friedman HR, Bruce CJ, Goldman-Rakic PS (1989) Resolution of metabolic columns by a double-label 2-DG technique: interdigitation and coincidence in visual cortical areas of the same monkey. J Neurosci 9:4111–4121.

Fujita I, Tanaka K, Ito M, Cheng, K (1992) Columns for visual features of objects in monkey inferotemporal cortex. Nature 360:343–346.

Geesaman BJ, Andersen RA (1996) The analysis of complex motion patterns by form/cue invariant MSTd neurons. J Neurosci 16:4716–4732.

Graziano MS, Andersen RA, Snowden, RJ (1994) Tuning of MST neurons to spiral motions. J Neurosci 14:54–67.

Hubel DH, Livingstone MS (1987) Segregation of form, color, and stereopsis in primate area 18. J Neurosci 7:3378–3415.

Hubel DH, Wiesel TN (1962) Receptive fields, binocular interaction and functional architecture in the cat's visual cortex. J Physiol 160:106–154.

Hubel DH, Wiesel TN (1968) Receptive fields and functional architecture of monkey striate cortex. J Physiol 195:215–243.

Hubel DH, Wiesel TN, Stryker MP (1977) Orientation columns in

macaque monkey visual cortex demonstrated by the 2-deoxyglucose autoradiographic technique. Nature 269:328–330.
Judge SJ, Richmond BJ, Chu FC (1980) Implantation of magnetic search coils for measurment of eye position: an improved method. Vision Res 20:535–538.
Juhler M, Diemer NH (1987) A method for ^{14}C and ^{3}H double-label autoradiography. J Cereb Blood Flow Metab 7:572–577.
Kennedy C, Des Rosiers M, Jehle JW, Reivich M, Sharp F, Sokoloff L (1975) Mapping of functional neural pathways by autoradiographic survey of local metabolic rate with ^{14}C deoxyglucose. Science 187:850–853.
Lagae L, Maes H, Raiguel S, Xiao DK, Orban GA (1994) Responses of macaque STS neurons to optic flow components: a comparison of areas MT and MST. J Neurophys 71:1597–1626.
Livingstone MS, Hubel DH (1981) Effects of sleep and arousal on the processing of visual information in the cat. Nature 291:554–561.
Livingstone MS, Hubel DH (1984) Anatomy and physiology of a color system in the primate visual cortex. J Neurosci 4:309–356.
Malonek D, Tootell RB, Grinvald A (1994) Optical imaging reveals the functional architecture of neurons processing shape and motion in owl monkey area MT. Proc Roy Soc Lond B 258:109–119.
Maunsell JH, Newsome WT (1987) Visual processing in monkey extrastriate cortex. Ann Rev Neurosci 10:363–401.
Maunsell J, van Essen DC (1983) Functional properties of neurons in middle temporal visual area of the macaque monkey. I. Selectivity for stimulus direction, speed, and orientation. J Neurophysiol 49:1127–1147.
Mitchison G (1992) Axonal trees and cortical architecture. Trends Neurosci 15:122–126.
Mountcastle VB (1957) Modality and topographic properties of single neurons of cat's somatic sensory cortex. J Neurophysiol 20:408–434.
Payne BR, Berman N, Murphy EH (1981) Organization of direction preferences in cat visual cortex. Brain Res 211:445–450.
Raiguel L, Orban G (1993) Speed and directional selectivity of macaque middle temporal neurons. J Neurophysiol 69:19–39.
Redies C, Diksic M, Evans AC, Gjedde A, Yamamoto YL (1987) Double-label autoradiographic deoxyglucose method for sequential measurement of regional cerebral glucose utilization. Neuroscience 22:601–619.
Robinson DA (1963) A method of measuring eye movement using a scleral search coil in a magnetic field. IEEE Trans Biomed Engng 10:137–145.
Sakata H, Shibutani H, Ito Y, Tsurugai K (1986) Parietal cortical neurons responding to rotatary movement of visual stimulus in space. Exp Brain Res 61:658–663.
Sanger TD (1988) Stereo disparity computation using Gabor filters. Biol Cybern 59:405–418.
Shadlen, MN, Newsome WT (1994) Noise, neural codes and cortical organization. Curr Opin Neurobiol 4:569–579.
Sokoloff L (1977) Relation between physiological function and energy metabolism in the central nervous system [Review]. J Neurochem 29:13–26.
Sokoloff L, Reivich M, Kennedy C, Des Rosiers MH, Patlak CS, Pettigrew KD, Sakurada O, Shinohara M (1977) The [^{14}C]deoxyglucose method for the measurement of local cerebral glucose utilization: theory, procedure, and normal values in the conscious and anesthetized albino rat. J Neurochem 28:897–916.
Swindale NV, Matsubara JA, Cynader MS (1987) Surface organization of orientation and direction selectivity in cat area 18. J Neurosci 7:1414–1427.
Tanaka K, Hikosaka K, Saito H, Yukie M, Fukada Y, Iwai E (1986) Analysis of local and wide-field movements in the superior temporal visual areas of the macaque monkey. J Neurosci 6:134–144.
Tolhurst DJ, Dean AF, Thompson ID (1981) Preferred direction of movement as an element in the organization of cat visual cortex. Exp Brain Res 44:340–342.
Tootell RBH, Born RT (1990) Patches and direction columns in primate area MT. Invest Ophthalmol (ARVO Abstr) 31:238.
Tootell RBH, Born RT (1991) Architecture of primate area MT. Soc Neurosci Abstr 17:524.
Tootell RBH, Silverman MS (1985) Two methods for flat-mounting cortical tissue. J Neurosci Methods 15:177–190.
Tootell RBH, Silverman MS, Switkes E, DeValois RL (1982) Deoxyglucose analysis of retinotopic organization in primate striate cortex. Science 218:902–904.
Tootell RBH, Born RT, Hamilton SL (1988a) Studies of primate visual cortex using double-label 2-dg and color autoradiograph. Soc Neurosci Abstr 14:897.
Tootell RBH, Hamilton SL, Silverman MS, Switkes E (1988b) Functional anatomy of macaque striate cortex. I. Ocular dominance, binocular interactions, and baseline conditions. J Neurosci 8:1500–1530.
Tootell RBH, Silverman MS, Hamilton SL, Switkes E, De Valois RL (1988c) Functional anatomy of macaque striate cortex. V. Spatial frequency. J Neurosci 8:1610–1624.
Tootell RBH, Born RT, Ash-Bernal R (1993) Columnar organization in visual cortex in non-human primates and man. In: Functional organization of the human visual system. Oxford: Pergamon Press.
Ungerleider LG, Desimone R (1986) Projections to the superior temporal sulcus from the central and peripheral field representations of V1 and V2. J Comp Neurol 248:147–163.